ADVANCES IN ATMOSPHERIC SCIENCES, VOL. 32, AUGUST 2015, 1143–1155

Study on Multi-Scale Blending Initial Condition Perturbations for a Regional Ensemble Prediction System

ZHANG Hanbin[1], CHEN Jing*[2], ZHI Xiefei[3], WANG Yi[4], and WANG Yanan[5]

[1]*College of Atmospheric Science, Nanjing University of Information Science and Technology, Nanjing* 210044
[2]*Numerical Weather Prediction Center, China Meteorological Administration, Beijing* 100081
[3]*Key Laboratory of Meteorological Disaster, Ministry of Education, Nanjing University of Information Science and Technology, Nanjing* 210044
[4]*Earth and Atmospheric Sciences, University of Nebraska Lincoln, Lincoln, Nebraska,* 68588*, USA*
[5]*Center of Meteorological Service of Zhejiang, Hangzhou* 310017

(Received 27 October 2014; revised 16 January 2015; accepted 22 January 2015)

ABSTRACT

An initial conditions (ICs) perturbation method was developed with the aim to improve an operational regional ensemble prediction system (REPS). Three issues were identified and investigated: (1) the impacts of perturbation scale on the ensemble spread and forecast skill of the REPS; (2) the scale characteristic of the IC perturbations of the REPS; and (3) whether the REPS's skill could be improved by adding large-scale information to the IC perturbations. Numerical experiments were conducted to reveal the impact of perturbation scale on the ensemble spread and forecast skill. The scales of IC perturbations from the REPS and an operational global ensemble prediction system (GEPS) were analyzed. A "multi-scale blending" (MSB) IC perturbation scheme was developed, and the main findings can be summarized as follows: The growth rates of the ensemble spread of the REPS are sensitive to the scale of the IC perturbations; the ensemble forecast skills can benefit from large-scale perturbations; the global ensemble IC perturbations exhibit more power at larger scales, while the regional ensemble IC perturbations contain more power at smaller scales; the MSB method can generate IC perturbations by combining the small-scale component from the REPS and the large-scale component from the GEPS; the energy norm growth of the MSB-generated perturbations can be appropriate at all forecast lead times; and the MSB-based REPS shows higher skill than the original system, as determined by ensemble forecast verification.

Key words: regional ensemble prediction system, spectral analysis, multi-scale blending, initial condition perturbations

Citation: Zhang, H. B., J. Chen, X. F. Zhi, Y. Wang, and Y. N. Wang, 2015: Study on multi-scale blending initial condition perturbations for a regional ensemble prediction system. *Adv. Atmos. Sci.*, **32**(8), 1143–1155, doi: 10.1007/s00376-015-4232-6.

1. Introduction

The errors related to initial conditions (ICs), numerical models, as well as the chaotic nature of the atmosphere (Lorenz, 1969), lead to great uncertainty in numerical weather prediction. It is desirable for numerical weather prediction to describe the evolution of the model atmosphere as a probability density function, rather than provide a deterministic result. It was in this context that ensemble prediction theory (Leith, 1974) was proposed. Ensemble prediction systems were originally implemented in the early 1990s at the National Centers for Environmental Prediction (NCEP; Toth and Kalnay, 1993) and at the European Center for Medium-Range Weather Forecasts (ECMWF; Molteni et al., 1996). Various ensemble perturbation schemes have since been developed to address the uncertainties in global ensemble prediction systems (GEPSs) related to ICs, such as singular vectors (SVs; Buizza and Palmer, 1995; Molteni et al., 1996), breeding growing modes (BGMs; Toth and Kalnay, 1993; 1997) and perturbed observation (Houtekamer et al., 1996; Buizza et al., 2005). Furthermore, with an increased emphasis on representing the analysis probability density function in the initial analysis state, the ensemble transform Kalman filter (ETKF; Wang and Bishop, 2003; Bowler et al., 2008; Ma et al., 2008), ensemble transform, and ensemble transform with rescaling (Wei et al., 2008), have been frequently used in recent years.

The development of regional ensemble prediction lags behind that of global ensemble prediction. Nevertheless, the need for regional ensemble prediction systems (REPSs) to provide mesoscale severe weather prediction is clear, so increasing numbers of related studies have been conducted (e.g., Du and Tracton, 2001; Grimit and Mass, 2002; Duan et

* Corresponding author: CHEN Jing
Email: chenj@cma.gov.cn

al., 2012). As the probability distributions of various sources of errors are complicated, it is difficult to address the uncertainties in the ICs, model physics and lateral boundary conditions (LBCs) of regional numerical weather prediction (Chen et al., 2004, 2005a). An important aspect of REPS research is exploring the effective methods to generate IC perturbations. One possibility in this regard is to apply dynamical downscaling to a GEPS (Marsigli et al., 2005; Frogner et al., 2006; Bowler et al., 2009). However, despite this method being attractive for its simplicity and good performance, small-scale uncertainties cannot be explicitly represented through downscaling (Wang et al., 2011). Other studies have generated IC perturbations for REPSs by using regional versions of traditional methods (i.e., BGMs, SVs, ETKF etc.) (Stensrud et al., 1999; Du et al., 2003; Chen et al., 2005b; Li et al., 2008; Wang et al., 2011; Zhang et al., 2014a), and demonstrated that these methods can generate some ensemble spread and benefit the forecast skill of the REPS. While it remains uncertain whether or not these regional IC perturbation generators are superior to dynamical downscaling (Bowler and Mylne, 2009; Saito et al., 2011), there is no doubt that they can produce more information on small/mesoscale uncertainties, and this information is particularly useful for the forecasting of high-impact weather, quantitative precipitation, and local severe convective weather (Chen et al., 2005b; Stensrud and Yussouf, 2007). However, when using these regional versions of traditional IC perturbation generators, it was found that the mismatches in the LBCs can be a significant source of spurious perturbations, and thus the use of a "blending" scheme was proposed (Wang et al., 2011; Caron, 2013; Du et al., 2014). This method can combine the small-scale component from the IC perturbations of a regional ensemble with the large-scale component from the IC perturbations of a global ensemble, and has proven to be effective in ameliorating the problem of mismatch in the LBCs (Caron, 2013).

The Numerical Weather Prediction Center of the China Meteorological Administration (CMA) has been routinely running a REPS since 2014. The system calculates IC perturbations by using a regional version of ETKF. Although this REPS has proven to be feasible in providing probabilistic forecasts of mesoscale phenomena, the system still faces several obstacles, such as a lack of ensemble spread, obvious systematic bias, and imperfect prediction of mesoscale uncertainty (Zhang et al., 2014b). Therefore, further improvement is needed. Bowler et al. (2009) reported that using downscaling, rather than the regional ETKF approach, to produce IC perturbations for REPSs can achieve better ensemble spread and forecast skill. As downscaling can create IC perturbations with more information at large scales, while regional perturbation generators can create IC perturbations with more information at small scales (Bowler and Mylne, 2009), questions arise as to whether the perturbation scale is an important factor, or to what extent different scale perturbations can affect the REPS' spread and forecast skill. Addressing these issues could lead to improvements in current REPSs.

In this study, we examine the impacts of perturbation scale on the ensemble spread and forecast skill of a REPS. Meanwhile, the scale characteristics of the IC perturbations generated by an operational ETKF are studied. We also explore the benefits of adding more large-scale information into the REPS IC perturbations, leading to the development of a multi-scale blending (MSB) perturbation method. The paper is structured as follows: section 2 introduces the model and data; section 3 compares the results of different numerical experiments that used different initial perturbation scale settings; and section 4 demonstrates the positive impacts of the MSB perturbation method on the ensemble spread and forecast skill of the REPS. A conclusion and discussion are provided in section 5.

2. Model and data

2.1. *The regional ensemble prediction system*

The REPS of the CMA, which has been running operationally since May 2014, was constructed based on the regional version of the Global/Regional Assimilation and Prediction Enhanced System (GRAPES) model (i.e., GRAPES_Meso; Chen and Shen, 2006). This REPS (referred to as GRAPES-REPS hereafter) aims to provide probabilistic forecasts of mesoscale severe weather, such as intense precipitation and strong convection, as well as the tracks and intensity of tropical cyclones.

2.1.1. *Operational configuration*

The GRAPES_Meso model runs on a regular latitude–longitude grid with a resolution of 0.15° in the horizontal direction and 33 levels in the vertical. The model domain of GRAPES-REPS is set to (15°–64.35°N, 70°–145.15°E) (Fig. 1), and the background data and LBCs are provided by a T639 global ensemble prediction system (T639-GEPS). GRAPES-REPS consists of 15 members, including a control run and 14 perturbed ensemble members, and is initiated at 0600, 1200, 1800 and 0000 UTC each day. Five variables (zonal wind u, meridional wind v, potential temperature θ, Exner pressure π, and specific humidity q) in the ICs are perturbed using the ETKF scheme. For each initiation time, the system provides 6 h forecast perturbations for the next

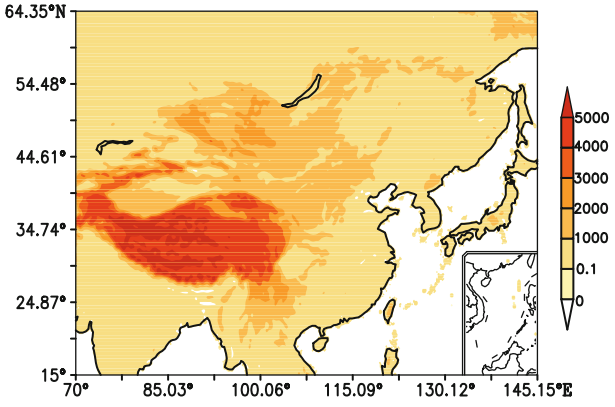

Fig. 1. GRAPES-REPS domain and model topography (units: m).

ETKF cycle; specifically, for the 1200 and 0000 UTC initiation times, the model integrates to 72 h to provide ensemble prediction products.

2.1.2. *Operational scheme*

GRAPES-REPS generates IC perturbations via the ETKF method, while the model uncertainty is represented by multi-physics. The LBCs of GRAPES-REPS are perturbed through coupling with T639-GEPS.

The ETKF scheme (Wang and Bishop, 2003), in generating IC perturbations, is based on the hypothesis that the forecast covariance matrices and analysis covariance matrices can be represented by forecast perturbations $\boldsymbol{X}_{\rm f}$ and analysis perturbations $\boldsymbol{X}_{\rm a}$. The relationship between $\boldsymbol{X}_{\rm a}$ and $\boldsymbol{X}_{\rm f}$ is established after solving the optimal data assimilation equation. As a result, the forecast perturbation can be transformed to the analysis perturbation through a transformation matrix $\boldsymbol{T}$:

$$\boldsymbol{X}_{\rm a} = \boldsymbol{X}_{\rm f} T \Pi \,, \tag{1}$$

where forecast perturbations are listed as columns in the matrix $\boldsymbol{X}_{\rm f}$ and analysis perturbations are listed as columns in the matrix $\boldsymbol{X}_{\rm a}$. $\boldsymbol{T}$ is the transformation matrix and Π is a scalar inflation factor to inflate the analysis perturbation amplitude so as to ensure that the 6 h forecast ensemble variance is consistent with the control forecast variance (Wang and Bishop, 2003; Wang et al., 2004).

The model uncertainty of GRAPES-REPS is represented by multi-physics (Houtekamer et al., 1996; Chen and Xue, 2009). GRAPES_Meso contains multiple physical process parameterizations, and different options for each physical process are provided. Since the microphysics and cumulus parameterization are closely related to precipitation, and the planetary boundary layer is critical for the transport of momentum and heat fluxes, the scheme of multi-physics is combining different options of the three processes randomly.

2.2. *Experimental data*

2.2.1. *The T639-based global ensemble prediction system*

The background states and LBCs of GRAPES-REPS are provided by T639-GEPS. The resolution of this GEPS is T639L60 (spectral triangular T639 with 60 vertical levels, corresponding to 30 km resolution), with ICs perturbed using BGMs. The BGM cycle interval is 12 h, initiated at 0000 and 0012 UTC each day with a forecast lead time of 15 days. A single control forecast is also initiated at 0006 and 0018 UTC to meet the requirements of GRAPES-REPS in terms of the background states and LBCs at these two initiation times. Model uncertainties are simulated using a stochastic physical parameterization scheme (Buizza et al., 1999).

2.2.2. *Data for verification*

The T639-GEPS analysis states corresponding to each forecast lead time are interpolated to a common regular $0.15^\circ \times 0.15^\circ$ grid to verify the variables at different pressure levels, while the precipitation is verified against observational accumulative precipitation from 2507 meteorological stations in China.

3. Numerical experiments with multi-scale IC perturbations

To investigate whether or not the perturbation scale is an important factor affecting the perturbation growth and forecast skill of the REPS, the results from a series of numerical experiments that used different IC perturbation scales are studied.

3.1. *Construction of IC perturbations with different scales*

A "scale selective perturbation generator", which can construct IC perturbations with a particular scale, was developed with the following steps:

Step 1: Generate a series of uniform random numbers r_i between -1.5 and 1.5 using a random number generator (Buizza et al., 1999).

Step 2: Divide the regular grid domain into small domains $(D_1, D_2, \ldots, D_i)$ of the same size (the size of the small domains corresponds to the required scale in a test), and then assign the random number r_i derived from Step 1 to the conjunctional grid points between the small domains as their values. Meanwhile, the values of grid points within the small domains are obtained through bilinear interpolation, and thereby a random number grid state characterized by a particular scale is formed, with values of all grids distributed smoothly.

Step 3: Generate seven (half of the number of perturbed members) two-dimensional random grid states via Step 2, and then multiply the random grid states by the statistical analysis error of the five variables (u, v, θ, π and q) at different model levels to obtain seven groups of perturbations for all variables at all levels.

Step 4: Add the seven groups of perturbations to (or subtract from) the IC of the control, and then the IC perturbations of the first (or last) seven of the 14 ensemble members are obtained. Meanwhile, the IC perturbations for the 14 perturbed members are positive–negative paired.

By using the "scale selective perturbation generator", three tests with different scale settings (namely, R1, R2 and R3) were conducted. The scales for the three tests are listed in Table 1. For all the tests in this section, the model configuration was the same as the operational run. A test period of 10 consecutive days (5–15 August 2012) was conducted. The ensembles were initiated at 1200 UTC on each day, with a forecast length of 72 h.

3.2. *Analysis of results*

The characteristics of different types of perturbations are

Table 1. Configuration of the IC perturbations for the three regional ensemble forecast tests.

Test	Perturbation scale	Size of small	Smoothed with bilinear interpolation?
R1	Smallest	1 grid space (about 15 km)	No
R2	Larger	20 grid spaces (about 300 km)	Yes
R3	Largest	70 grid spaces (about 1000 km)	Yes

investigated. Here, we employ a total energy norm, which is appropriate for weather forecasting and data assimilation (Palmer et al., 1998). For one grid located at (i, j, k), the energy of the perturbation is computed from winds and temperature using the approximate energy norm defined as

$$E(i,j,k) = \frac{1}{2}[u'^2(i,j,k) + v'^2(i,j,k)] + \frac{c_p}{T_r} T'^2(i,j,k) \ , \quad (2)$$

where u', v' and T' are wind and temperature perturbations, c_p is the specific heat and T_r is the reference temperature (Wang and Bishop, 2003; Wei et al., 2006).

Figure 2 shows the horizontal distribution of the vertically averaged IC perturbation energy norm for the first ensemble member. It can be seen that, although the amplitudes of the three types of perturbations are similar, there are remarkable differences in the horizontal distribution pattern. The perturbation for R1 is structured with very small scale, while the perturbation scale for the R2 scheme is increased and the number of perturbation centers is reduced, and the R3 scheme presents perturbations with the largest scale and fewest centers.

To examine the vertical distributions and evolutions of the three types of perturbations, we averaged the energy norm of all grid points at each level. Figure 3 shows the resulting vertical distribution profiles of the perturbation energy norm for the R1, R2 and R3 ensembles. It is clear that the perturbation growth is quite different for the three schemes. The energy norm at all levels in the R1 ensemble is larger than that of the other two at the initial time (00 h). For the R1 scheme, the energy norm at 200 hPa can reach 2.3 J kg^{-1}, while for R2 and R3 the corresponding values are about 2.15 J kg^{-1}. For the 6 h forecast, the R1 scheme perturbations at most levels are sharply reduced to less than 1 J kg^{-1}, whereas for the R2 and R3 ensembles the perturbations exhibit growth. As the forecast lead time increases, the perturbations of the three ensembles grow gradually. The R3 perturbations show the largest growth, as the 36 h energy magnitude at 250 hPa is 3.6 J kg^{-1}. For the R2 ensemble, the perturbation growth is relatively smaller; the 36 h energy value at 250 hPa is 2.9 J kg^{-1}. The perturbations for R1 are smallest, as the energy at all levels is even smaller than that at the initial time. For the total energy norm of all three schemes demonstrated in Fig. 3, it seems that the differences at the upper levels are dominated by kinetic energy, while the differences at the lower levels are dominated by internal energy (not shown). This is because the kinetic energy has larger magnitude at the upper levels and the internal energy has larger magnitude at the lower levels.

The above result indicates that perturbations with larger scale exhibit more adequate perturbation growth. The reason for this behavior might be that larger scale perturbations can easily form "organized structure", and perturbations with this "organized structure" can easily evolve into "flow dependent" perturbations that can develop well with the atmospheric flow (Toth and Kalnay, 1993). Meanwhile, smaller scale perturbations are more like inertial gravity waves and are generally decaying (e.g. Lacarra and Talagrand, 1988), and thus the perturbation growth would be constrained. This result indicates that the spread growth of the regional ensemble is sensitive to the perturbation scale, with large-scale perturbations more prone to growth.

Verification of the three ensembles was performed (not shown). Results averaged over 10 days showed remarkable

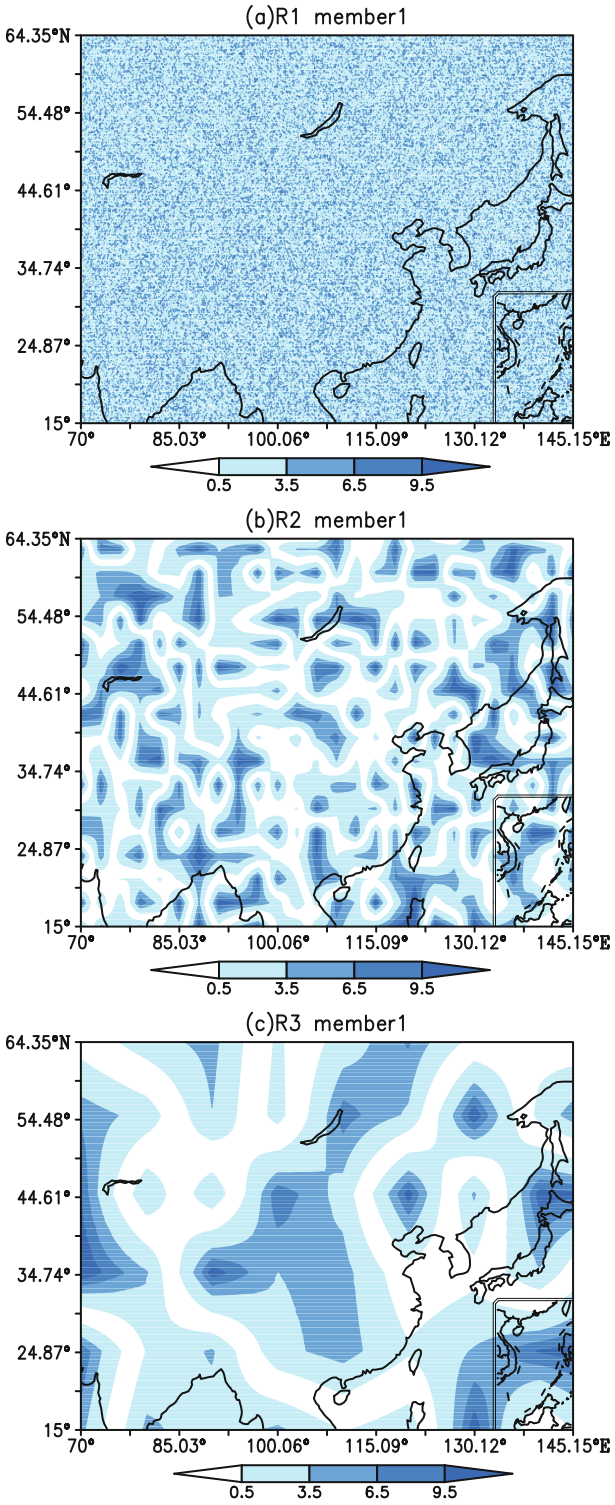

Fig. 2. Horizontal distribution of vertically averaged IC perturbation energy norm (units: J kg^{-1}) for the first member of three ensemble schemes of (a) R1, (b) R2 and (c) R3.

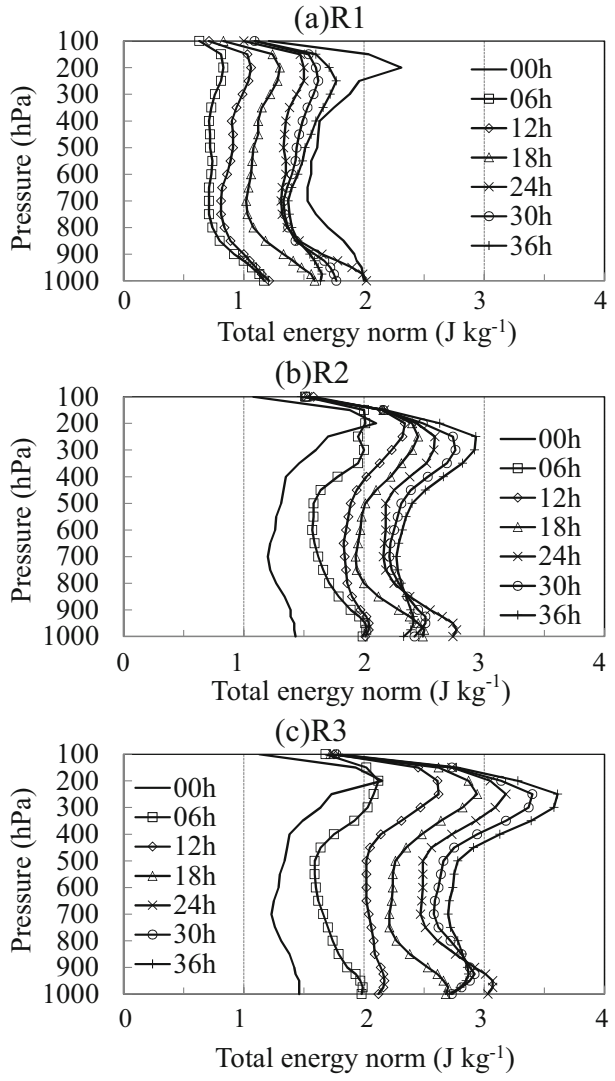

Fig. 3. Vertical distributions of the perturbation energy norm (units: J kg^{-1}) of the (a) R1 scheme, (b) R2 scheme and (c) R3 scheme. Different lines denote different forecast lead times.

differences in the spread and root-mean-square error (RMSE). R3 maintained the largest spread at all forecast lead times, followed by R2 and then R1. This indicates that perturbations with larger scale favor the growth of ensemble spread. As the current REPS is known for its lack of spread (Zhang et al., 2014a), the amplified spread due to the enlarged perturbation scale could also lead to RMSE reduction, thus enabling large-scale perturbations to produce a much better ensemble forecast. The improved probability verification scores due to amplified perturbation scale also supported this conclusion.

4. Multi-scale blending experiment

4.1. *Power spectra analysis of IC perturbations derived from T639-GEPS and GRAPES-REPS*

Because of the effect of perturbation scale on ensemble forecast spread and forecast skill, as reported in section 3, it is necessary to investigate the scale characteristics of GRAPE-REPS IC perturbations generated by the ETKF. The scale characteristics of T639-GEPS IC perturbations are also studied as comparison. The power spectra of IC perturbations were calculated for both T639-GEPS and GRAPE-REPS using a 2-dimemsional discrete cosine transform (2D-DCT, Denis et al., 2002), which is suitable for spectral analysis and spectral filtering of data in a limited area.

For a two-dimensional field $f(i,j)$ of N_i by N_j grid points, the direct and inverse 2D-DCT are defined as

$$F(m,n) = \beta(m)\beta(n) \sum_{i=0}^{i=N_i-1} \sum_{j=0}^{j=N_j-1} f(i,j) \times \cos\left[\pi m \frac{(i+1/2)}{N_i}\right] \cos\left[\pi n \frac{(j+1/2)}{N_j}\right] , \quad (3)$$

and

$$f(i,j) = \sum_{m=0}^{m=N_i-1} \sum_{n=0}^{n=N_j-1} \beta(m)\beta(n)F(m,n) \times \cos\left[\pi m \frac{(i+1/2)}{N_i}\right] \cos\left[\pi n \frac{(j+1/2)}{N_j}\right] , \quad (4)$$

respectively, with

$$\beta(m) = \begin{cases} \sqrt{\dfrac{1}{N_i}} & m = 0 \\ \sqrt{\dfrac{2}{N_i}} & m = 1,2,\ldots,N_i-1 \end{cases} , \quad (5)$$

and

$$\beta(n) = \begin{cases} \sqrt{\dfrac{1}{N_j}} & n = 0 \\ \sqrt{\dfrac{2}{N_j}} & n = 1,2,\ldots,N_j-1 \end{cases} . \quad (6)$$

Here, $f(i,j)$ is the field value at grid point (i,j), and $F(m,n)$ is the spectral coefficient corresponding to the (m,n) dimensional wave numbers. A 2D-DCT applied to a physical field $f(i,j)$ of N_i by N_j values can produce an N_i by N_j array of $F(m,n)$ real spectral coefficients.

In this section, the 2D-DCT is used to compute the power spectra from two-dimensional perturbation fields. In two dimensions, the perturbation state $p(i,j)$ with N_i by N_j grid points, for a variable at one level of a member, is defined as

$$p(i,j) = a(i,j) - a_{\rm ctl}(i,j) , \quad (7)$$

where $a(i,j)$ is an ensemble member's IC state and $a_{\rm ctl}(i,j)$ is the control analysis state. According to Eq. (3) the two-dimensional perturbation fields $p(i,j)$ can be decomposed into a spectral field forming an N_i by N_j two-dimensional array, $P(m,n)$. Since our goal in generating spectra is to evaluate the perturbation of two-dimensional fields as a function of spatial scales, each two-dimensional wave number pair (m,n) needs to be associated with a single-scale parameter; namely, a wavelength λ. For a rectangular domain of N_i by N_j, we

have

$$\lambda = \frac{2\Delta}{\sqrt{\frac{m^2}{N_i^2} + \frac{n^2}{N_j^2}}}, \tag{8}$$

where Δ is the grid point spacing.

Figure 4a shows all-member averaged power spectra of 500 hPa temperature IC perturbations as a function of wavelength, with T639-GEPS downscaled to the same domain and resolution as GRAPES-REPS. We can see that the power of GRAPES-REPS perturbations is greater than that of T639-GEPS perturbations at wavelengths less than 1100 km. In particular, for scales less than 60 km (around two grid lengths of T639 global model), there is no power for T639-GEPS perturbations, and this is mainly because these scales cannot be resolved by the global model. Whereas, for scales over 1100 km, more power can be found in the global ensemble, as the maximum power can reach 40 K^2 (corresponding to the wavelength of 5000 km), while the maximum value for the regional ensemble can only reach 20 K^2 (corresponding to the wavelength of 3200 km). According to the analysis in section 3, the more power at large scales may lead to a larger spread of the global ensemble, and thus if the large-scale component of global ensemble perturbations is introduced into the regional ensemble, we believe that this may be beneficial to the spread and forecast skill of the REPS.

4.2. *Construction methodology for the multi-scale blending IC perturbations*

Based on the above analysis, it is highly desirable to obtain the IC perturbations that contain the optimal components of the regional ensemble and global ensemble. Thus, we explore an MSB perturbation approach. The MSB-generated IC perturbations can be partitioned into two parts: a small-scale component and a large-scale component, in which the terms "small" and "large" are reflective of the relative relationship between the two components, and are not defined by exact values. The small-scale component is provided by the regional ensemble IC perturbations computed from the ETKF, while the large-scale component is provided by the global ensemble IC perturbations. A digital filter was used to conduct the scale selection.

4.2.1. *Introduction to the filter*

A low-pass filter for separating horizontal meteorological fields into different scales can be easily designed based on the aforementioned 2D-DCT (Denis et al., 2002). The direct application of the 2D-DCT to a physical field produces an array of spectral coefficients in which the spatial scales are related to the two-dimensional wave numbers (or wavelength). Low-pass filtering can easily be performed by applying a transfer function onto the two-dimensional spectral coefficients. This is done by multiplying the spectral coefficient array by a transfer function array with values between 0 and 1. In this study, a gradually varying transfer function with a soft cutoff was used to avoid Gibbs phenomena (Wang et al., 2014). The transfer function used for the cutoff transition zone follows a squared cosine. Figure 5 shows an example of such a transfer function, also commonly called the amplitude response function of the filter. For this low-pass filter, all scales shorter than "w1" km were removed and all scales larger than "w2" km were preserved. Thereafter, an inverse transform [Eq. (4)] was applied to rebuild the filtered physical field.

4.2.2. *Filter scheme for IC perturbations of T639-GEPS and GRAPES-REPS*

To conduct the scale filter for T639-GEPS and GRAPES-REPS, we needed to choose appropriate critical wavelengths, "w1" and "w2", for the transition zone. We first divided the

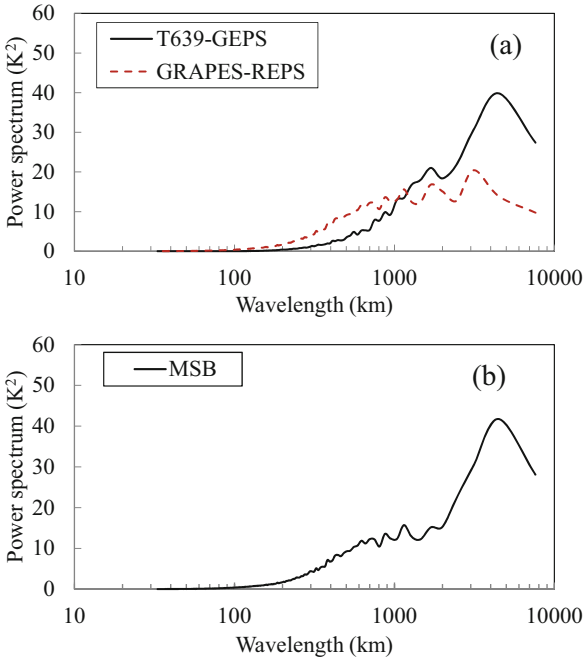

Fig. 4. All-member averaged power spectra of 500 hPa temperature IC perturbations as a function of wavelength for (a) T639-GEPS and GRAPES-REPS; and (b) MSB.

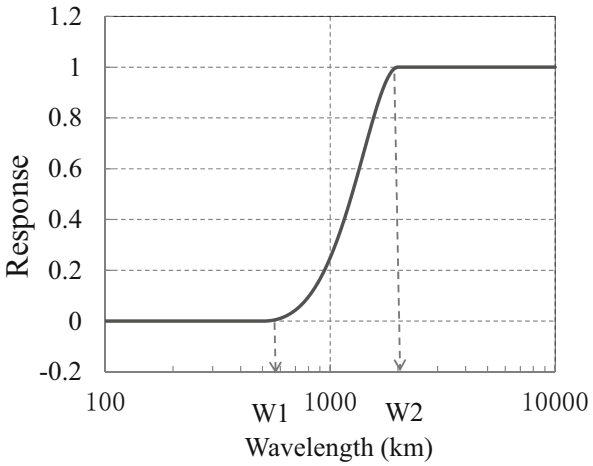

Fig. 5. Response of the 2D-DCT low-pass filter.

scales that can be represented by both the GEPS and REPS into several intervals: 60–120 km, 120–240 km, 240–480 km, 480–960 km, 960–1920 km, and 1920–3840 km, with the smallest wavelength (60 km) able to be represented by T639-GEPS and the longest wavelength (3840 km) by GRAPES-REPS (7530 km in the latitudinal direction and 4950 km in the longitudinal direction). By comparing the one-month averaged power-scale curves (similar to Fig. 4a) of the global ensemble and the regional ensemble, we can identify the intersection scale (at scales larger than the intersection scale, the global ensemble contains more power, while at scales smaller than the intersection scale, the regional ensemble contains more power). The intersection scales for different variables and different levels are listed in Table 2. In order to obtain the optimal combination that contains the relatively more powerful part of the two ensembles, the critical wavelengths (scales) for different variables and levels were determined according to the corresponding intersection scales listed in Table 2. Hence, for a particular variable at a given level, the transition zone was determined by the aforementioned scale interval within which the intersection scale lays.

After the transition zones for all variables at all levels were determined, the 2D-DCT low-pass filter was performed directly to the downscaled T639-GEPS IC perturbations. This enabled the scales larger than w2 to remain untouched, while the scales smaller than w1 to be removed completely.

In order to obtain the small-scale component from the regional ensemble IC perturbations, we also applied the 2D-DCT low-pass filter to the GRAPES-REPS IC perturbations, with the critical wavelengths the same as those used in the T639-GEPS filtering. We then subtracted the filtered large-scale component from the original IC perturbation fields to obtain the small-scale perturbation components.

4.2.3. *Method for blending the filtered perturbations*

The large-scale component of the T639-GEPS IC perturbations (denoted as T639-LS) and the small-scale component of the GRAPES-REPS IC perturbations (denoted as ETKF-SS, because the IC generation method is the ETKF) were linearly combined with equal weight, such that the MSB IC perturbations were obtained by

$$\mathrm{IP_{MSB}} = \mathrm{IP_{T639\text{-}LS}} + \mathrm{IP_{ETKF\text{-}SS}} \ , \tag{9}$$

where $\mathrm{IP_{MSB}}$ denotes the MSB IC perturbations.

Figure 6 shows 850 hPa u wind perturbation for T639-LS, ETKF-SS and MSB. It is clear that, after the filtering process,

Table 2. Intersection scales of the IC perturbation power spectra for GRAPES-REPS and T639-GEPS.

Level (hPa)	Zonal wind (u)	Meridional wind (v)	Potential temperature (θ)	Exner pressure (π)	Specific humidity (q)
150	80 km	80 km	350 km	500 km	120 km
200	150 km	150 km	500 km	1360 km	180 km
300	230 km	230 km	800 km	1670 km	410 km
400	250 km	250 km	950 km	1810 km	540 km
500	540 km	540 km	1140 km	1990 km	720 km
600	770 km	770 km	1540 km	2380 km	610 km
700	850 km	850 km	1790 km	2500 km	760 km
800	950 km	950 km	1990 km	3100 km	1230 km
850	1150 km	1150 km	2500 km	3520 km	1120 km
925	1500 km	1500 km	2500 km	4300 km	1610 km

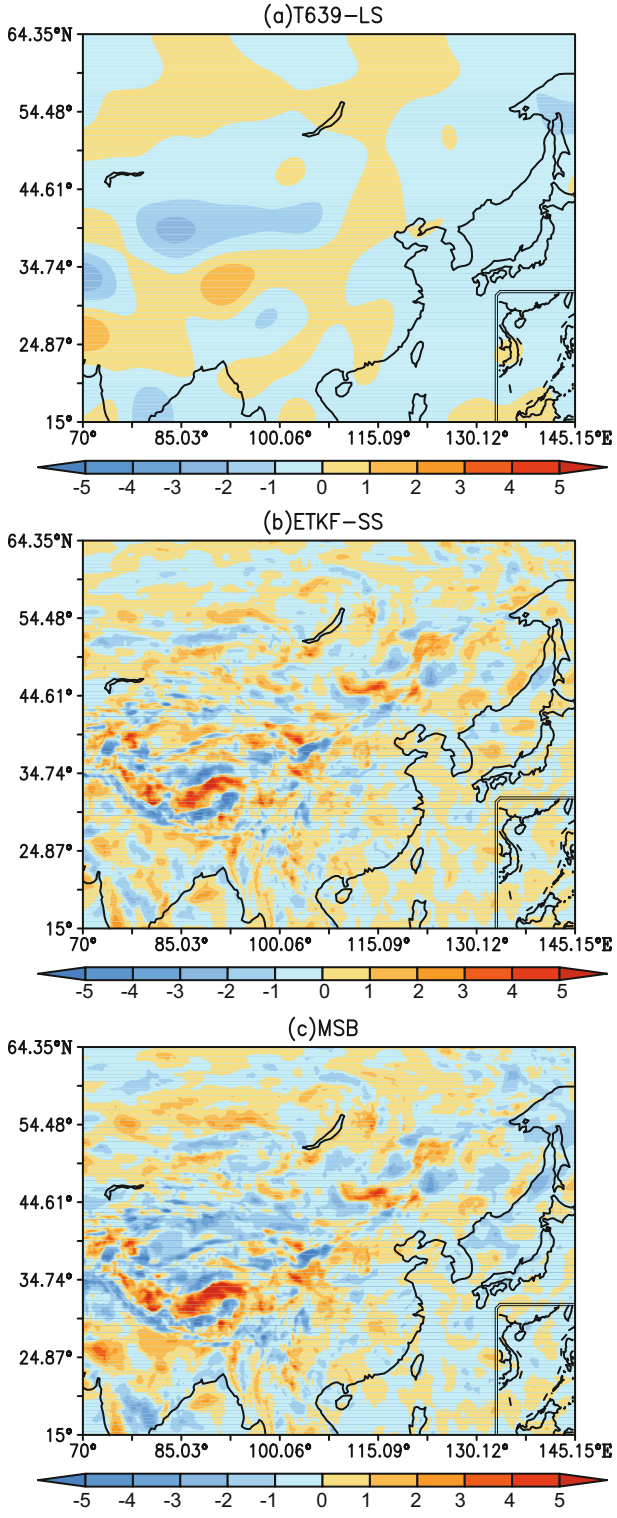

Fig. 6. IC perturbations of 850 hPa zonal wind for (a) T639-LS, (b) ETKF-SS and (c) MSB.

only the large-scale component remains in the T639-LS perturbation states, while the small-scale component remains in the ETKF-SS perturbation states. As a combination of the two, the MSB perturbation states include information at all scales.

4.3. *Experiment results*

The MSB scheme was tested in the operational GRAPES-REPS environment and compared with the operational ETKF scheme. The experimental model configurations for both schemes were the same, and the experiment was carried out over a period of one month (August 2012).

4.3.1. *Spectral analysis of MSB perturbations*

The power spectrum of the MSB perturbations is evaluated. From Fig. 4b, we can see that the MSB perturbations of 500 hPa temperature present significant power not only at large scales but also at small scales. Compared with Fig. 4a, the MSB perturbations contain the same amount of power as GRAPES-REPS at small scales, while exhibiting the same characteristics as T639-GEPS at large scales, with the maximum power value of 43 K^2.

4.3.2. *Comparison of MSB perturbations with ETKF perturbations*

The operational test results of GRAPES-REPS posed an issue that the ETKF generated perturbations exhibited slow growth. Indeed, the problem of "under-dispersion" of an ensemble system is often encountered in today's REPS studies. This section presents the characteristics of the MSB perturbations and perturbation evolution. Perturbations derived from the ETKF are also presented as a comparison.

Figure 7 shows the energy norm profile at all levels for 0–36 h forecast lead times. For the initial time (00 h), the ETKF ensemble perturbation energy norm has two maximum values: one located at the upper levels of 150 hPa, with a value of 2.2 J kg^{-1}, and the other located at the bottom level, with a value of 2.17 J kg^{-1}. We speculate that this maximum value at the bottom mainly lies underground, and that these are spurious perturbations that come from interpolation, especially in the plateau area. Thus, these perturbations attenuate rapidly within short forecast lead times, and then start to grow gradually. For the MSB, the 00 h energy norm distribution at the upper levels is different from that of the ETKF, with a maximum value of 3 J kg^{-1} at 250 hPa. This is mainly due to the introduction of the large-scale component from GEPS. For levels above 850 hPa, the energy norm is significantly larger than that of the ETKF ensemble, while for levels lower than 850 hPa, the MSB energy norm profile is similar to that of the ETKF.

We also note that the most remarkable growth level of the ETKF perturbations is between 200 and 300 hPa, as the 36 h energy norm at 250 hPa can reach 4 J kg^{-1}. For MSB, the most obvious energy norm growth can also be found at 250 hPa, where the 36 h energy norm is 4.4 J kg^{-1}, which is more than that of the ETKF perturbations. The growth of MSB perturbations at other levels can also exceed that of the ETKF

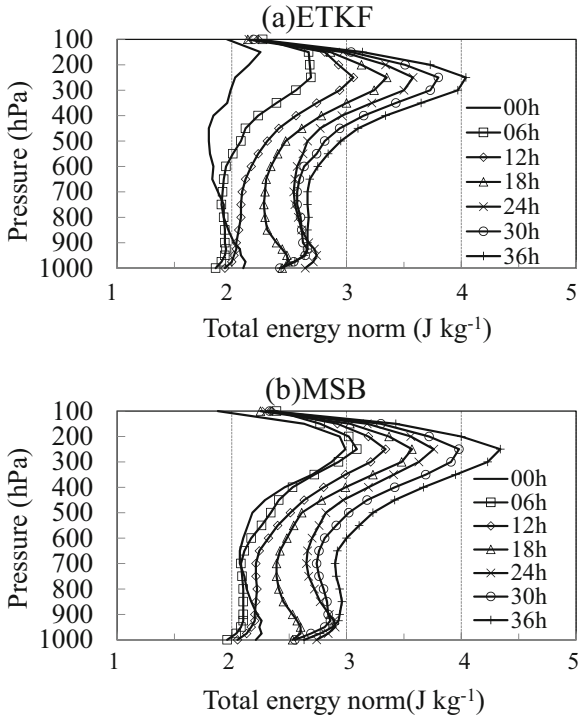

Fig. 7. Vertical distribution of ensemble mean total energy (units: J kg^{-1}), with different lines denoting different forecast lead times: (a) ETKF scheme; (b) MSB scheme.

perturbations. Since a rapid amplification of analysis error can lead to large forecast errors, it is desirable for an ensemble to contain perturbations representative of likely analysis errors that can grow quickly (Wang and Bishop, 2003). For the ETKF perturbations in Fig. 7a, the maximum energy norm level does not correspond well to the fastest growth level. In other words, the most powerful perturbation within the ETKF ensemble subspace does not point to the most rapid growth direction, whereas the MSB method can adjust the energy norm distribution through adding more perturbations to the levels where energy can grow quickly, and thus higher growth rates can be found within the MSB ensemble perturbation subspace.

4.3.3. *Statistical verification*

An attempt was made to verify the performance of the MSB-based REPS and ETKF-based REPS using various score measures, including the RMSE of ensemble mean, ensemble spread, continuous rank probability score (CRPS), and percentage of outliers.

Figures 8a–c show the one month averaged RMSE of the ensemble mean and the ensemble spread of 500 hPa temperature (T500), 500 hPa wind speed (WS500) and 10m *u* wind (U10m), for ETKF and MSB, respectively. For all variables presented, the MSB shows an improved RMSE–spread relationship compared to that of the ETKF, given that the RMSE is smaller while the spread is larger for the MSB ensemble. Similar results can also be observed for other variables at different levels, indicating that the large-scale component from

the GEPS can benefit the growth of ensemble spread and improve the ensemble mean forecast quality.

Figures 8d–f show the CRPSs of T500, W500 and U10m, respectively. The CRPS has a negative orientation, the smaller the better (Hersbach, 2000). It is clear that MSB performs better than the ETKF, and such an advantage of MSB over the ETKF increases with forecast lead time. CRPS verification on other variables produced similar results (not shown).

Another measure of statistical reliability is the percentage of outliers. This is a statistic of the number of cases when the verifying analysis at any grid point lies outside the whole ensemble. A more reliable ensemble should have a smaller percentage of outliers (Wang et al., 2011). It is evident that MSB has fewer outliers than ETKF for all the variables (Figs. 8g–i), indicating a greater tendency for the observation to lie inside the MSB ensemble.

From the above analyses, we find an overall improvement of MSB over ETKF, either for upper-air or near-surface variables. While the improvement of MSB compared to the ETKF is not overly substantial, in the context that enhancing the performance of a REPS through the initial perturbations is recognized a challenging issue, even a slight improvement is desirable. Therefore, these one-month averaged results do indeed indicate the superiority of the MSB method.

4.3.4. *A typical heavy rainfall case*

A typical heavy rainfall case in summer 2012 was studied. Both ensembles were initiated at 1200 UTC 19 August 2012, with all model configurations the same as those in the operational setting.

Figure 9 shows the observation, the heavy precipitation probability and the spread for 24 h accumulated precipitation from 0000 UTC 20 to 0000 UTC 21 August 2012. As shown in the observation (Fig. 9a), this case was characterized by a large precipitation area over central China, with the rainfall

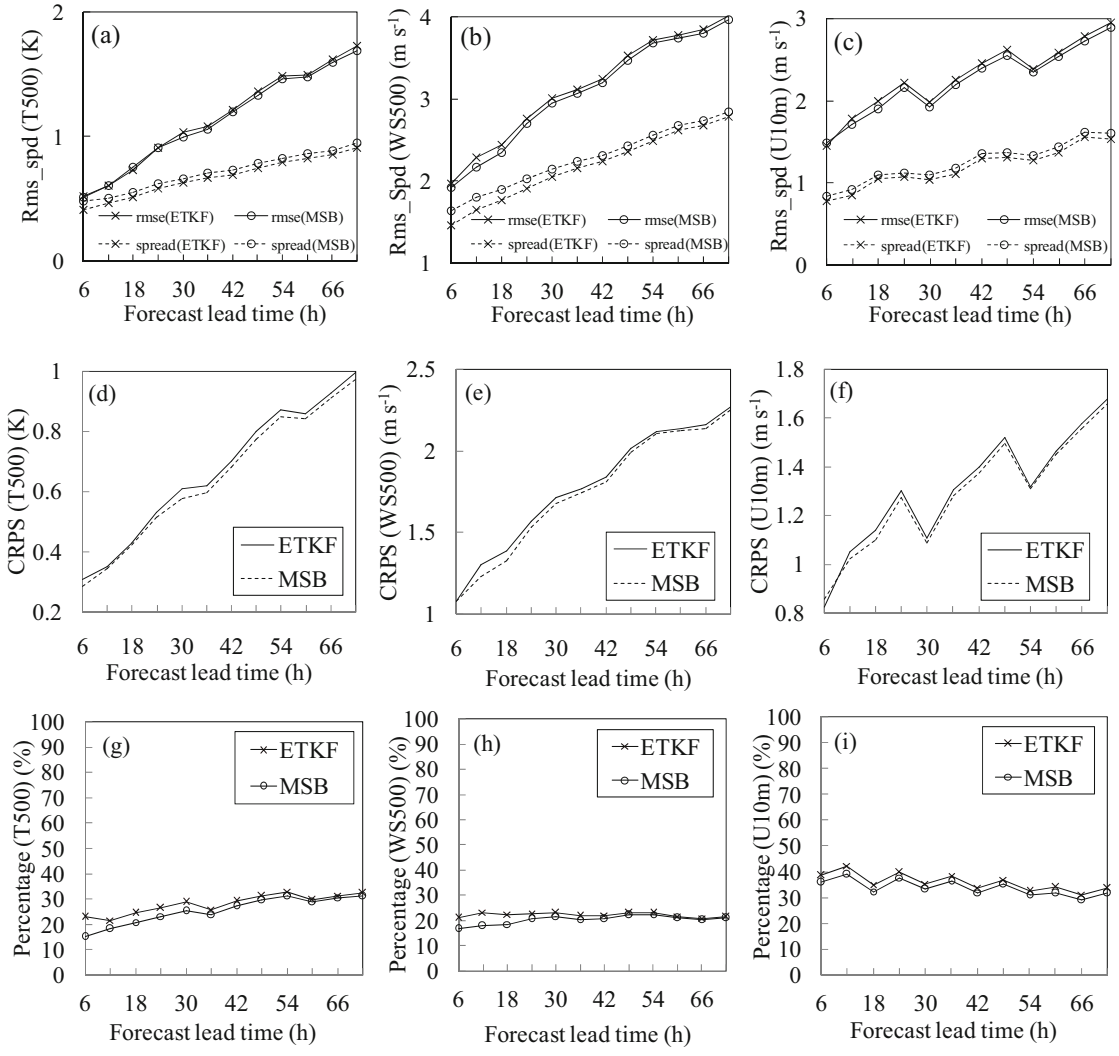

Fig. 8. Ensemble verification results for ETKF and MSB. Panels (a–c) show the RMSE of ensemble mean and spread for T500, WS500 and U10m respectively; panels (d–f) show the CRPS for T500, WS500 and U10m, respectively; panels (g–i) show the percentage of outliers for T500, WS500 and U10m, respectively.

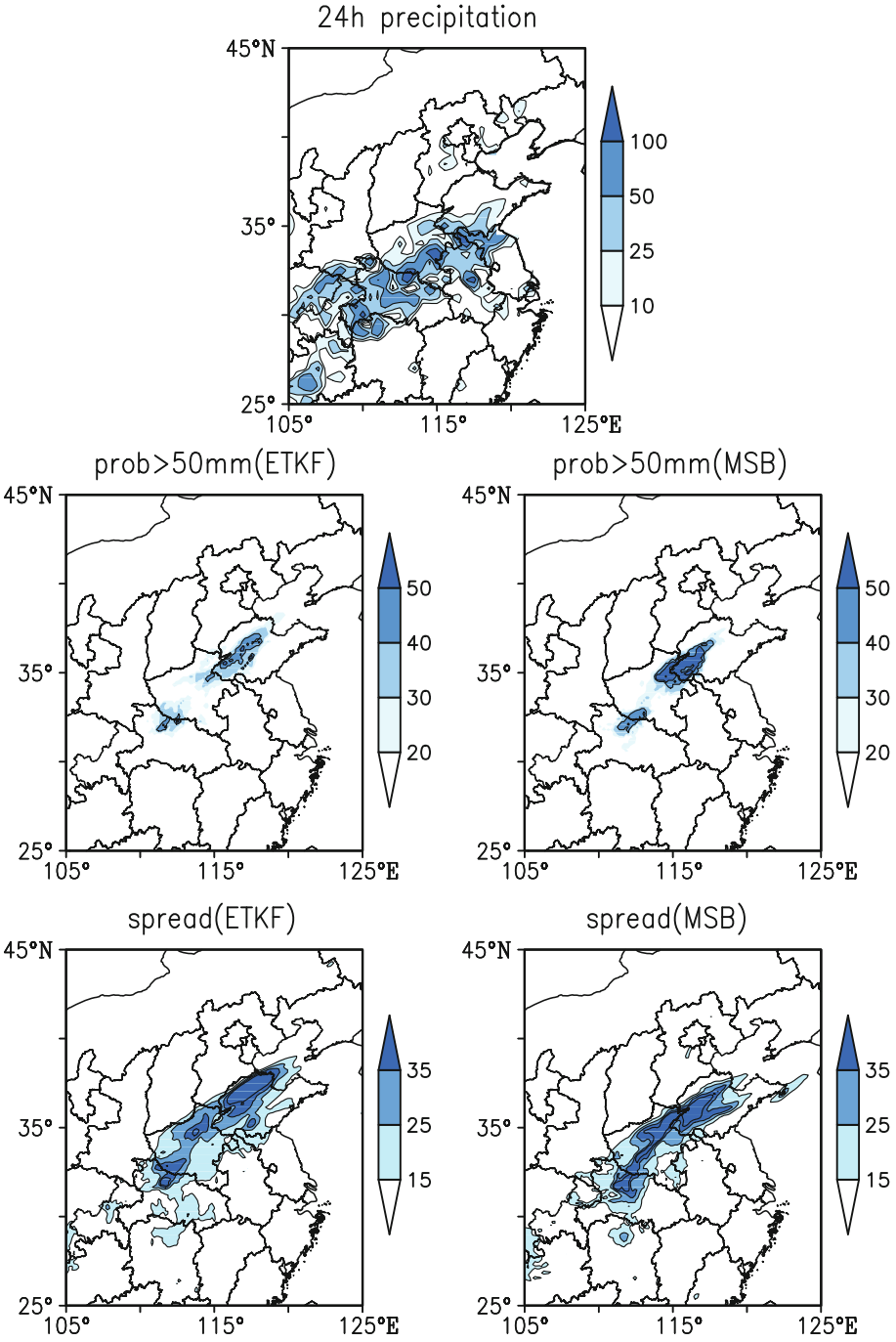

Fig. 9. Observational state, heavy precipitation probability and spread for 24 h accumulative precipitation: (a) observation (units: mm); (b) precipitation probability over 50 mm (units: %) for the ETKF ensemble forecast (all magnitudes are shown as shaded, with magnitudes over 40% contoured); (c) as in (b) but for the MSB; (d) spread of 24 h accumulative precipitation (units: mm) for the ETKF ensemble forecast; (e) as in (d) but for the MSB.

band exhibiting a west–east pattern. Figures 9b and c present the probability of 24 h accumulated precipitation over 50 mm. All of the probability magnitudes are represented by shading, with magnitudes over 40% highlighted by contours. For the ETKF ensemble (Fig. 9b), the area with magnitudes of greater than 25% covers the northwest part of Shandong, and the high probability region (contoured) exhibits a northeast shift relative to the observed precipitation center. Also apparent is an area with probability greater than 25% located over the north coastal region of Shandong, whereas the observed precipitation was less than 5 mm in this region. Furthermore, an area with probability less than 25% can be seen over the center of Henan, but the observation shows there was a precipitation center at the same location, with a maximum value

over 90 mm. For MSB (Fig. 9c), the locations and ranges of high probability areas are closer to the observation. For example, the range of probability over 40% near the border of Shandong and Henan is enlarged, and an area with probability over 25% emerged at the center of Henan, corresponding well with the observation.

The spread of the ETKF ensemble (Fig. 9d) places great emphasis on the northern part of Shandong, where the observed rain band was not located, and thus such a large precipitation spread at that location is meaningless. Whereas, the spread of the MSB ensemble (Fig. 9e) has large values over the west of Shandong, which is close to the observed rainfall band. This larger spread with better locations effectively increases the chances of MSB ensemble members to capture the location of heavy rainfall accurately.

The performances of the two ensembles with respect to their precipitation forecasts were examined by computing the one month averaged Brier Score (BS) and Area of Relative Operating Characteristic (AROC), which are appropriate for measuring the probability forecast skill of an ensemble in terms of the quantitative precipitation forecast. The BS measures the mean squared difference between the predicted probability and the observed occurrence of an event, producing a value of between zero and one, with a smaller value indicating better performance. The AROC denotes the relative relationship between the hit rate and the false alarm rate for a threshold of an event. A higher AROC means a higher hit rate and better probability forecast, and vice versa. Figure 10a presents the BS for both the ETKF and MSB, with a forecast lead time of 36 h. The MSB ensemble shows better performance than the ETKF ensemble at all precipitation magnitudes. For heavy rain greater than 50 mm, the BS of the MSB ensemble (0.013) exhibits 50% improvement over that of the ETKF (0.028). Figure 10b presents the AROC for both ensembles with a forecast lead time of 36 h. For this AROC index, the MSB ensemble has a higher score not only for light and moderate rain but also for intense rain. Therefore, this result supports the conclusion obtained from the BS analyses.

Since the spatial distribution of heavy precipitation is sensitive to the atmospheric flow, more information on MSB perturbations at larger scales can help to improve the representation of atmospheric circulation factors in the model, thereby improving the spatial distribution forecast of heavy rainfall. This case study clearly demonstrates that combining the small-scale component of the regional ensemble and the large-scale component of the global ensemble is an effective way to improve the quality of probabilistic precipitation forecasts.

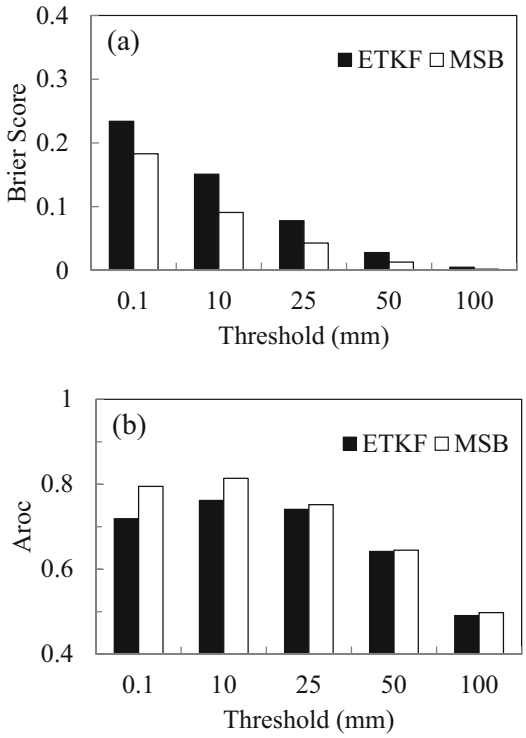

Fig. 10. Comparison of the probabilistic precipitation forecast skills of the ETKF and the MSB in terms of (a) BS and (b) AROC.

5. Conclusions and discussion

To improve the operational regional ensemble prediction system GRAPES-REPS, three issues were investigated in this study: (1) whether the scale of perturbations is an important factor affecting the ensemble spread and ensemble forecast skill; (2) what the scale characteristics of GRAPES-REPS are; and (3) whether the REPS's skill can be improved by adding more large-scale information to the IC perturbations. Experiments were conducted to test the impact of perturbation scale on ensemble spread growth and forecast skill; the scale characteristics of GRAPES-REPS were investigated and compared with that of T639-GEPS; and an MSB IC perturbation scheme was tested. The key findings of the study can be summarized as follows:

A "scale selective perturbation generator" was designed to generate IC perturbations characterized by a particular scale. Three sets of experiments were carried out with different perturbation scales, and the results showed that the spread growth rate of GRAPES-REPS is sensitive to the scale of IC perturbations. Overall, perturbations with larger scale exhibit a higher rate of spread growth and better skill.

The power spectra of IC perturbations from T639-GEPS and GRAPES-REPS were analyzed and compared using a 2D-DCT. Results indicated that perturbations derived from the global ensemble show more power at larger scales, while the regional ensemble perturbations contain more power at smaller scales. The fact that the ETKF generated regional ensemble perturbations lacking large-scale information led us to consider if adding more large-scale information from a GEPS would improve the REPS's performance.

An MSB IC perturbation scheme was developed. This method takes advantage of both the large-scale component of global ensemble perturbations and the small-scale compo-

nent of ETKF-generated IC perturbations, with the two components obtained using a 2D-DCT filter and linearly combined with equal weight. The MSB and ETKF schemes were compared through a series of experiments in the operational environment. Results showed that, compared to the ETKF, the MSB scheme can generate IC perturbations with more power at larger scales, and the power at smaller scales is also preserved. The total energy norm of MSB perturbations can maintain appropriate growth at all forecast lead times. Verification showed a higher skill of the MSB ensemble than the ETKF ensemble. A comparison between MSB and ETKF in terms of precipitation forecasting also showed better performance of the MSB ensemble. All of the results indicated that introducing a large-scale component into the regional ensemble IC perturbations can enhance the REPS's spread and forecast skill, basically because it is this introduced large-scale information that the regional ensemble otherwise lacks. The findings of this study are useful for directing future upgrades of the current REPS.

The effect of the MSB method on the mismatch in the LBCs of GRAPES-REPS was not investigated in the present study because the domain for GRAPES-REPS covers a wide area including the whole of China, and so the spurious gravity waves caused by the mismatch in the LBCs take little account of the IC perturbations within the whole domain. Further experiments that take account of the mismatch in the LBCs in a small-domain ensemble will be carried out in the future.

As the MSB method is better at representing large-scale uncertainties relative to the regional ETKF, we speculate that the advantages of MSB over ETKF might be greater in cases with stronger synoptic forcing, but less so in cases with weaker synoptic forcing. We plan to investigate more cases in the future to verify this hypothesis.

Acknowledgements. This study was supported by the National Natural Science Foundation of China (Grant No. 91437113), the Special Fund for Meteorological Scientific Research in the Public Interest (Grant Nos. GYHY201506007 and GYHY201006015), the National 973 Program of China (Grant Nos. 2012CB417204 and 2012CB955200) and the Scientific Research & Innovation Projects for Academic Degree Students of Ordinary Universities of Jiangsu (Grant No. KYLX_0827). The authors would like to thank Dr. DU Jun at the National Centers for Environmental Prediction and Dr. WANG Yong at the Central Institute for Meteorology and Geodynamics of Austria for their constructive comments and suggestions.

REFERENCES

Bowler, N. E., and K. R. Mylne, 2009: Ensemble transform Kalman filter perturbations for a regional ensemble prediction system. *Quart. J. Roy. Meteor. Soc.*, **135**, 757–766.

Bowler, N. E., A. Arribas, K. R. Mylne, K. B. Robertson and S. E. Beare, 2008: The MOGREPS short-range ensemble prediction system. *Quart. J. Roy. Meteor. Soc.*, **134**, 703–722.

Bowler, N. E., A. Arribas, S. E. Beare, K. R. Mylne, and G. J. Shutts, 2009: The local ETKF and SKEB: Upgrades to the MOGREPS short-range ensemble prediction system. *Quart. J. Roy. Meteor. Soc.*, **135**, 767–776.

Buizza, R., and T. N. Palmer, 1995: The singular-vector structure of the atmospheric global circulation. *J. Atmos. Sci.*, **52**, 1434–1456.

Buizza, R., M. Milleer and T. N. Palmer, 1999: Stochastic representation of model uncertainties in the ECMWF ensemble prediction system. *Quart. J. Roy. Meteor. Soc.*, **125**, 2887–2908.

Buizza, R., P. L. Houtekamer, Z. Toth, P. Pellerin, M. Z. Wei, and Y. J. Zhu, 2005: A comparison of the ECMWF, MSC, and NCEP global ensemble prediction systems. *Mon. Wea. Rev.*, **133**, 1076–1097.

Caron, J. F., 2013: Mismatching perturbations at the lateral boundaries in limited-area ensemble forecasting: A case study. *Mon. Wea. Rev.*, **141**, 356–374.

Chen, D. H., and X. S. Shen, 2006: Recent progress on GRAPES research and application. *Journal of Applied Meteorological Science*, **17**, 773–777. (in Chinese)

Chen, J., and J. S. Xue, 2009: Heavy rainfall ensemble prediction: Initial condition perturbation vs multi-physics perturbation. *Acta Meteorologica Sinica*, **23**(1), 53–67.

Chen, J., J. Xue, H. Yan, 2004: The impact of non-adiabatic physics on mesoscale short-range heavy rainfall prediction. *Acta Meteorological Sinica*, **18**(1), 51–72.

Chen, J., J. Xue, H. Yan, 2005a: The uncertainty of heavy rainfall of South China and experiments of ensemble prediction. *Acta Meteorological Sinica*, **19**(1), 1–18.

Chen, J., J. S. Xue, and H. Yan, 2005b: A new initial perturbation method of ensemble mesoscale heavy rain prediction. *Chinese Journal of Atmospheric Sciences*, **29**, 717–726. (in Chinese)

Denis, B., J. Côté, and R. Laprise, 2002: Spectral decomposition of two-dimensional atmospheric fields on limited-area domains using the discrete cosine transform (DCT). *Mon. Wea. Rev.*, **130**, 1812–1829.

Du, J., and M. S. Tracton, 2001: Implementation of a real-time short range ensemble forecasting system at NCEP: An update. *Preprints*, 9*th Conference on Mesoscale Processes*, Ft. Lauderdale, Florida, Amer. Meteor. Soc., 355–356.

Du, J., G. DiMego, M. S. Tracton, and B. Zhou, 2003: NCEP short-range ensemble forecasting (SREF) system: Multi-IC, multi-model and multi-physics approach. Research Activities in Atmospheric and Oceanic Modeling, J. Côté, Ed., Rep. 33, CAS/JSC Working Group Numerical Experimentation (WGNE), WMO/TD-No. 1161, 5. 09–5. 10.

Du, J., G. DiMego, B. B. Zhou, D. Jovic, B. Ferrier, B. Yang, S. Benjamin, 2014: NCEP regional ensembles: Evolving toward hourly-updated convection-allowing scale and storm-scale predictions within a unified regional modeling system. 26*th Conf. on Weather Analysis and Forecasting and* 22*nd Conf. on Numerical Weather Prediction*, Atlanta, GA, Amer. Meteor. Soc., 1–6 Feb. 2014, paper J1. 4.

Duan, Y. H., and Coauthors, 2012: An overview of the Beijing 2008 Olympics Research and Development Project (B08RDP). *Bull. Amer. Meteor. Soc.*, **93**, 381–403.

Frogner, I. -L., H. Haakenstad, T. Iversen, 2006: Limited-area ensemble predictions at the Norwegian Meteorological Institute. *Quart. J. Roy. Meteor. Soc.*, **132**, 2785–2808.

Grimit, E. P., and C. F. Mass, 2002: Initial results of a mesoscale short-range ensemble forecasting system over the Pacific Northwest. *Wea. Forecasting*, **17**, 192–205.

Hersbach, H., 2000: Decomposition of the continuous ranked

probability score for ensemble prediction systems. *Wea. Forecasting*, **15**, 559–570.

Houtekamer, P. L., L. Lefaivre, J. Derome, H. Ritchie, and H. L. Mitchell, 1996: A system simulation approach to ensemble prediction. *Mon. Wea. Rev.*, **124**, 1225–1242.

Lacarra, J. F., and O. Talagrand, 1988: Short-range evolution of small perturbations in a barotropic model. *Tellus A*, **40A**, 81–95.

Leith, C. E., 1974: Theoretical skill of Monte Carlo forecasts. *Mon. Wea. Rev.*, **102**, 409–418.

Li, X. L., M. Charron, L. Spacek, and G. Candille, 2008: A regional ensemble prediction system based on moist targeted singular vectors and stochastic parameter perturbations. *Mon. Wea. Rev.*, **136**, 443–462.

Lorenz, E. N., 1969: Predictability of a flow which possesses many scales of motion. *Tellus*, **21**, 289–307.

Ma, X. L., J. S. Xue, and W. S. Lu, 2008: Preliminary study on ensemble transform Kalman filter-based initial perturbation scheme in GRAPES global ensemble prediction. *Acta Meteorologica Sinica*, **66**(4), 526–536. (in Chinese)

Marsigli, C., F. Boccanera, A. Montani, and T. Paccagnella, 2005: The COSMO-LEPS mesoscale ensemble system: Validation of the methodology and verification. *Nonlinear Processes in Geophysics*, **12**, 527–536.

Molteni, F., R. Buizza, T. N. Palmer, and T. Petroliagis, 1996: The ECMWF ensemble prediction system: Methodology and validation. *Quart. J. Roy. Meteor. Soc.*, **122**, 73–119.

Palmer, T. N., R. Gelaro, J. Barkmeijer and R. Buizza, 1998: Singular vectors, metrics, and adaptive observations. *J. Atmos. Sci.*, **55**, 633–653.

Saito, K., M. Hara, H. Seko, M. Kunii, and M. Yamaguchi, 2011: Comparison of initial perturbation methods for the mesoscale ensemble prediction system of the Meteorological Research Institute for the WWRP Beijing 2008 Olympics Research and Development Project (B08RDP). *Tellus A*, **63**, 445–467.

Stensrud, D. J., and N. Yussouf, 2007: Reliable probabilistic quantitative precipitation forecasts from a short-range ensemble forecasting system. *Wea. Forecasting*, **22**, 3–17.

Stensrud, D. J., H. E. Brooks, J. Du, M. S. Tracton, and E. Rogers, 1999: Using ensembles for short-range forecasting. *Mon. Wea. Rev.*, **127**, 433–446.

Toth, Z., and E. Kalnay, 1993: Ensemble forecasting at NMC: The generation of perturbations. *Bull. Amer. Meteor. Soc.*, **74**, 2317–2330.

Toth, Z., and E. Kalnay, 1997: Ensemble forecasting at NCEP and the breeding method. *Mon. Wea. Rev.*, **125**, 3297–3319.

Wang, X. G., and C. H. Bishop, 2003: A comparison of breeding and ensemble transform Kalman filter ensemble forecast schemes. *J. Atmos. Sci.*, **60**, 1140–1158.

Wang, X. G., C. H. Bishop, and S. J. Julier, 2004: Which is better, an ensemble of positive–negative pairs or a centered spherical simplex ensemble? *Mon. Wea. Rev.*, **132**, 1590–1605.

Wang, Y., M. Bellus, J. F. Geleyn, X. L. Ma, W. H. Tian, and F. Weidle, 2014: A new method for generating initial condition perturbations in a regional ensemble prediction system: Blending. *Mon. Wea. Rev.*, **142**, 2043–2059.

Wang, Y., and Coauthors, 2011: The Central European limited-area ensemble forecasting system: ALADIN-LAEF. *Quart. J. Roy. Meteor. Soc.*, **137**, 483–502.

Wei, M. Z., Z. Toth, R. Wobus, and Y. J. Zhu, 2008: Initial perturbations based on the ensemble transform (ET) technique in the NCEP global operational forecast system. *Tellus A*, **60**, 62–79.

Wei, M. A., Z. Toth, R. Wobus, Y. J. Zhu, C. H. Bishop and X. G. Wang, 2006: Ensemble Transform Kalman Filter-based ensemble perturbations in an operational global prediction system at NCEP. *Tellus A*, **58**, 28–44.

Zhang, H. B., J. Chen, X. F. Zhi, K. J. Long and Y. N. Wang, 2014a: Design and comparison of perturbation schemes for GRAPES_Meso based ensemble forecast. *Transactions of Atmospheric Sciences*, **37**, 276–284. (in Chinese)

Zhang, H. B., J. Chen, X. F. Zhi, Y. L. Li and Y. Sun, 2014b: Study on the application of GRAPES regional ensemble prediction system. *Meteorological Monthly*, **40**, 1076–1087. (in Chinese)